Int. J. High Technology Ceramics **2** (1986) 47–63

Mechanical Property Evaluation at Elevated Temperature of Sintered β-Silicon Carbide

M. J. Slavin and G. D. Quinn

Ceramics Research Division, Army Materials Technology Laboratory, Watertown, Massachusetts 02172, USA

SUMMARY

The mechanical properties at room and elevated temperature of sintered β-silicon carbide were evaluated. Testing included room temperature flexural strength, flexural stress rupture at 1200°C, and stepped temperature stress rupture (STSR) experiments. Fractographic examination identified the strength limiting flaw populations. Properties measured on this material are typical of commercial grades of sintered silicon carbide.

1. INTRODUCTION

Silicon-based ceramics have considerable potential for structural applications in heat engines and other energy conversion devices. This study is part of an on-going Department of Energy project to screen the mechanical properties of new materials for heat engine applications.

This report presents findings on a commercially available sintered β-silicon carbide manufactured by the General Electric Co. In 10 years of development this material has evolved from a hot-pressed laboratory grade material to a commercial sintered product.[1–7] It is fabricated from a submicrometer β-silicon carbide powder with small additions (~0·5 wt% each) of boron and carbon, and is sintered in a reducing atmosphere at approximately 2100°C. The boron promotes diffusion while the carbon acts to reduce possible oxide phases (silicon dioxide) and retard grain growth. The sintered product often contains some α-phase silicon carbide

Int. J. High Technology Ceramics 0267-3762/86/$03·50

as a result of phase transformation during sintering. This latter process is dependent upon impurities and sintering conditions and can be very sensitive to conditions of powder preparation, processing, and densification.[3] The presence of the α-phase is not desired because it can manifest itself as large tabular grains that can limit strength.

Earlier studies have suggested that the laboratory hot-pressed and sintered β-silicon carbide materials have excellent high temperature properties up to 1500°C including creep and slow crack growth resistance[8–10] and strength retention.[1,4,9,10] These favorable properties, coupled with the complex shape capabilities of sintering, suggest that β-silicon carbide is a promising heat engine grade ceramic. The purpose of this study was to verify these properties in the commercial form of the material.

2. MATERIAL

The sintered β-silicon carbide was supplied by the General Electric Company's Manufacturing Division, Houston, Texas in the form of eight 50·8 × 50·8 × 12·7 mm tiles in March 1984. Four of these tiles were machined into flexure specimens according to MIL-STD-1942(MR)[11] specimen configuration 'B'. Specimen size was 3·0 × 4·0 × 44·5 mm with a 45° chamfer along the four long edges. Chamfer depths were inadvertently machined to approximately 0·28 mm which is greater than the 0·15 ± 0·05 mm the standard requires. Although this causes only a 1·25% decrease in the cross-sectional area, the strengths reported in this study (based on elastic theory with a rectangular cross-section) are 3·4% lower than if the chamfer were within the prescribed limits.

The average bulk density of the tiles was 3·12 Mg m^{-3} with a standard deviation of 0·03 and is in close agreement with the 3·12 Mg m^{-3} reported by the manufacturer. The elastic modulus and Poisson's ratio as measured via the sonic method were 395 GPa and 0·17, respectively.

The ultrasonic longitudinal wave propagation time C-scan is a powerful characterization tool. The time C-scan shows spatial variation of wave propagation times through the tile thickness with a resolution of ±1 ns. If a tile has constant thickness, the C-scan can be interpreted as a longitudinal velocity C-scan. Figure 1 is a C-scan of a 50·8 × 50·8 × 12·7 mm tile of β-silicon carbide and, allowing for wave distortion near the edges, had a variation in wave propagation time of approximately 5% from the edge to the center of the tile. The Appendix gives an analysis of the C-scan in which the relationship between the tile's thickness, elastic modulus, Poisson's ratio and density as they pertain to the longitudinal wave velocity is evaluated.

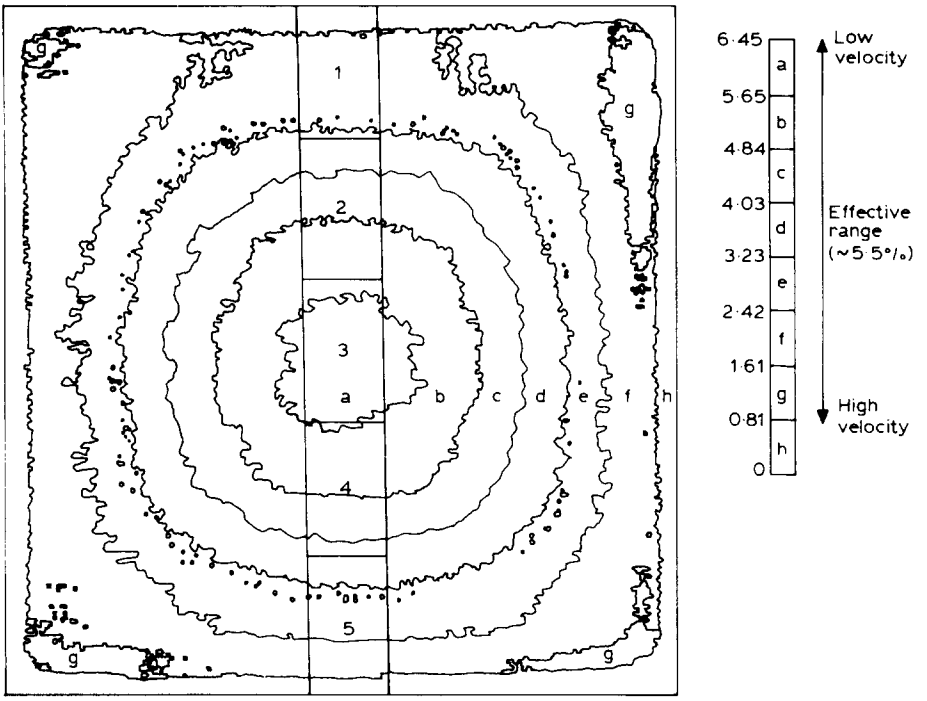

Fig. 1. Time-of-flight C-scan for the sintered β-silicon carbide using a 10 MHz undamped transducer.

The increase in the wave propagation time from the edge to the center of the tile is due to (in order of importance): an increase in thickness, a decrease in elastic modulus, and a decrease in Poisson's ratio. The density, which decreases toward the tile's center, decreases the wave propagation time.

A quantitive analysis of the metallic impurities is given in Table 1. A polished section showing the material porosity (~3%) is shown in Fig. 2. Figure 3 shows the same section etched with boiling Murakami's reagent to delineate the grain boundaries.[6] Tabular grains commonly associated

TABLE 1
Impurity or Additive Content of the Sintered β-Silicon Carbide

Impurity element/wt%[a]												
Al	*B*	*Ca*	*Co*	*Cr*	*Cu*	*Fe*	*Mg*	*Mn*	*Ni*	*Ti*	*Zr*	*V*
0·008	0·5	0·017	—[b]	0·005	0·005	0·003	0·002	~0·001	0·002	0·004	0·16	—[b]

[a] Determined by emission spectroscopy.
[b] Not detected.

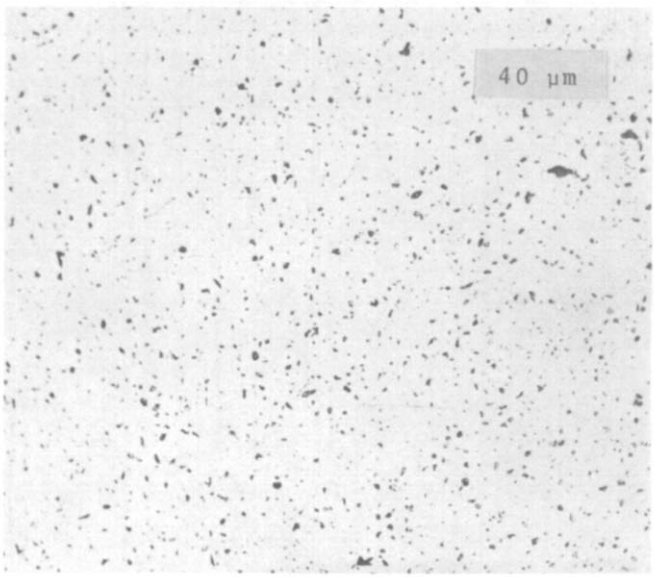

Fig. 2. Polished section of a specimen of β-silicon carbide showing the distribution of porosity.

Fig. 3. Etched section of a specimen showing grain size distribution. Note the long tabular α-grains.

with the α-phase of silicon carbide[1–5] are readily apparent. X-ray diffraction of the silicon carbide showed that the majority of the material is β-silicon carbide with a small percentage of the α-phase and a trace amount of graphite. In a parallel study being carried out at MTL[12] for non-heat engine applications, a 152·4 × 76·2 × 12·7 mm tile had an identical X-ray diffraction pattern and a very similar microstructure (larger α-grains).

3. PROCEDURE

Microhardness testing was performed on a mounted and polished specimen with a load of 19·6 N. Using both Vicker's and Knoop indenters, 10 indentations each were made with a standard microhardness indenter (Miniload II, Leitz, FRG). Fracture toughness was estimated from crack lengths emanating from Vicker's indentations at loads of 19·6 N, 24·9 N, and 34·3 N, using a standard microhardness indenter (Tukon Tester FB, Wilson Mechanical Instrument Co. Inc., New York).

Room temperature flexural testing was used to establish a reference strength and to characterize the strength limiting flaws. A universal testing machine (Model TT-DL, Instron Corp., Canton, Massachusetts) was used with four-point fixtures in accordance with MIL-STD-1942(MR).[11] The spans were 40·0 mm and 20·0 mm and the crosshead speed was 0·5 mm/min. The relative humidity was 35% at 23°C.

The 1200°C flexural stress rupture experiments were carried out in air in several identical test furnaces. These furnaces were constructed with firebrick and employed silicon carbide heating elements as the heat source.[13] Four-point bend fixtures, machined from hot-pressed silicon carbide and having fixed bearing spans of 38·1 mm and 19·0 mm, were used. A simple deadweight lever system applied the load into the furnace. The temperature inside the furnace was allowed to stabilize for 5 min prior to loading. Additional details of this procedure are given in Ref. 14.

A stepped temperature stress rupture (STSR)[15] program was used to quickly screen the material while stressed to a range of temperatures that it may be subjected to in an engine environment. This program assesses where creep or static fatigue may be a problem. The furnace arrangement and loading procedure are identical to the stress rupture tests. The program starts at 1000°C when the load is applied. After 24 h, if the specimen survives, the temperature is raised within approximately 0·5 h to 1100°C. This cycle continues for 1200°C, 1300°C, and 1400°C, but at 1400°C, the specimen cycle time is 72 h. In the event of a failure the furnace is shut down. An arrow labeled with the applied stress denotes the time of failure on the STSR plot.

Specimens that survived the stress rupture or STSR tests were unloaded prior to cool-down. This was done to minimize frictional forces at the knife edges due to unequal specimen-fixture contractions. The survivors were then tested at room temperature to determine the retained strength. They were mounted in the room temperature fixture such that the most highly stressed zone in the high temperature test was again loaded in a tensile manner. Note that the room temperature fixtures have slightly larger inner and outer spans than the high temperature fixtures.

4. RESULTS

The Vicker's indentations produced an average hardness of 23·9 GPa with a standard deviation of 0·4 GPa and the Knoop indentations an average hardness of 20·9 GPa with a standard deviation of 0·3 GPa. This is somewhat lower than the HV9·8 N of 28·0 GPa reported in Ref. 7 but a little higher than the average HK9·8 N of 20·1 GPa with a standard deviation of 0·8 GPa (60 indentations) reported in Ref. 12.

The fracture toughness values were measured from Vicker's indentations and evaluated using the Marshall–Evans formulation.[16] A minimum of five 'good' indentation patterns were obtained for each of the three loads. Some problems with spall and cracks not radiating from the corners were observed. A 'good' indentation pattern consisted of at least three of the four cracks starting from the corners and extending straight from the indent and no spall. Table 2 indicates that the K_{Ic} values averaged 2·8 MPa $m^{0.5}$. This is somewhat lower than other reported values: 3·0 MPa $m^{0.5}$ (double torsion),[17] 3·3 MPa $m^{0.5}$ (single edge notch beam),[12] and 3·1 MPa $m^{0.5}$ (controlled flaw in flexure).[18]

Thirty room temperature four-point fast fracture specimens were tested and had an average flexure stress of 346 MPa with a standard deviation of 34 MPa. This average is appreciably less than values for the laboratory-prepared three-point flexure specimens in Ref. 6, is somewhat less than the 440 MPa four-point results reported in Refs 9 and 10, is also less than

TABLE 2
Fracture Toughness, K_{Ic}, for Varying Indent Loads

Load/N	*Number of indents (n)*	K_{Ic}/*MPa* $m^{0.5}$
19·5	5	2·82
29·4	6	2·81
34·3	6	2·78

Average K_{Ic} = 2·8 MPa $m^{0.5}$, with a standard deviation of 0·2.

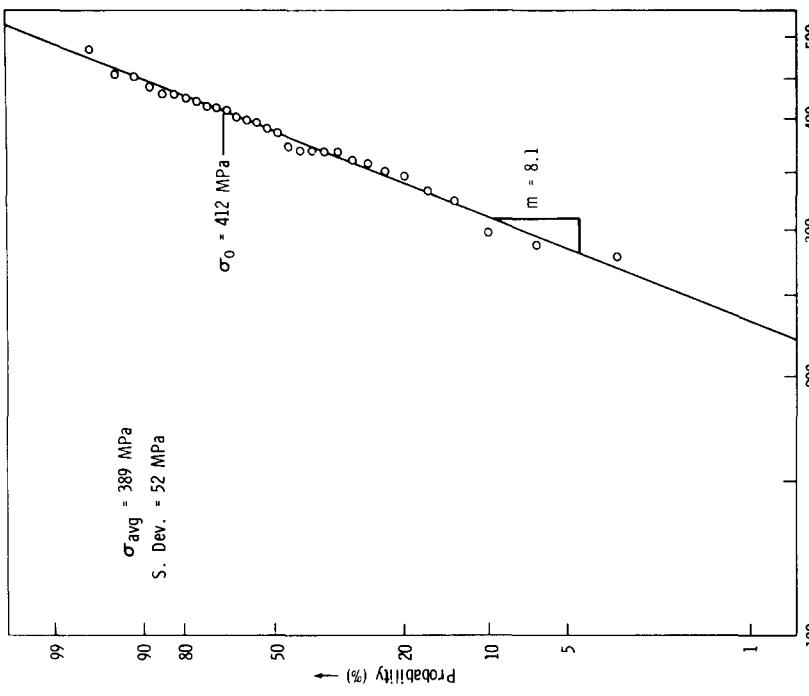

Fig. 5. Weibull plot for the parallel study underway at AMMRC.[12]

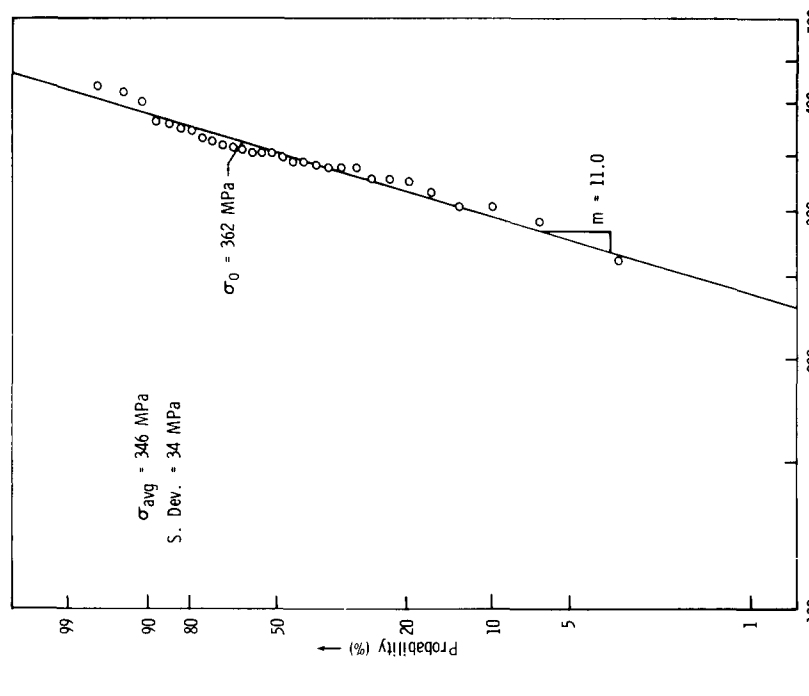

Fig. 4. Weibull plot for the reference flexural strength for this study.

the three-point value of 533 MPa in Ref. 7, but is quite consistent with the four-point value of 389 MPa with a standard deviation of 52 MPa in Ref. 12.

A two-parameter Weibull modulus was determined by a least square fitted line through the strength data when plotted on a standard Weibull format (see Fig. 4). The ranking percentage is $p = i/(N+1)$, where i is the ith data point and N is the total number of specimens. The Weibull modulus, which is the slope of the line, is 11·0 and has a correlation coefficient of 96·5%. Figure 5 is a Weibull plot for the strength data from the parallel study underway at MTL[12] for non-heat engine applications. The Weibull modulus is 8·1 with a correlation coefficient of 98·8%. These moduli are consistent with the reported value of 8 to 15 in Ref. 7.

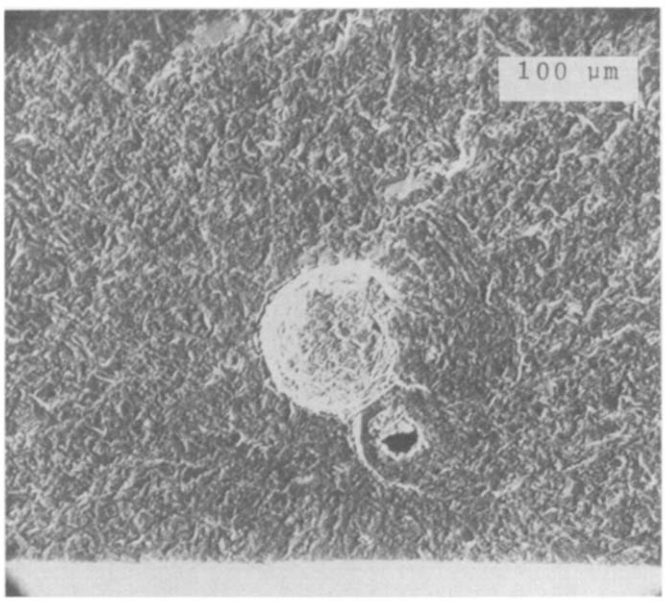

Fig. 6. Fracture surface of a control sample that failed due to the agglomerate and pore: 352 MPa.

All specimens were subjected to a fractographic examination up to a magnification of about 100×. Typical fracture surfaces were then photographed and prepared for SEM examination. The strength-limiting flaws common to the room temperature flexure specimens were: agglomerates and porous zones either at the surface or distributed within the volume (Fig. 6); a few large grains and pores (Fig. 7); and an occasional processing crack (Fig. 8). Thus, although the Weibull plot implies a single flaw population, there are, in fact, several.

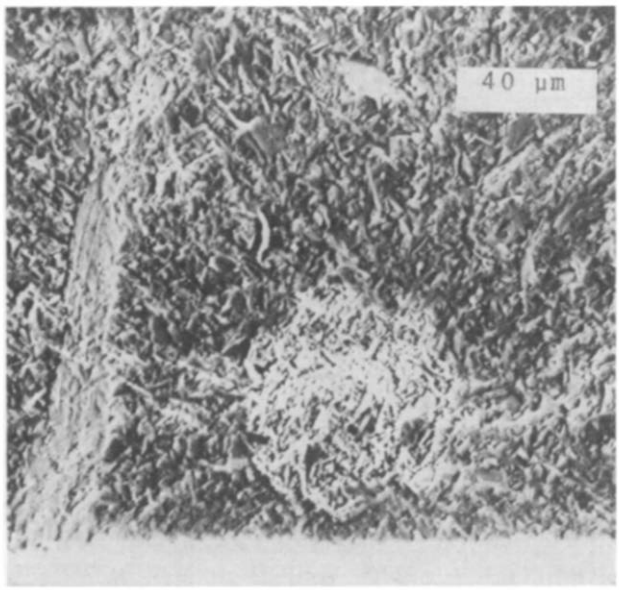

Fig. 7. Fracture surface of a control sample: 356 MPa. The strength-limiting flaw is the combination of the porous area and the grain.

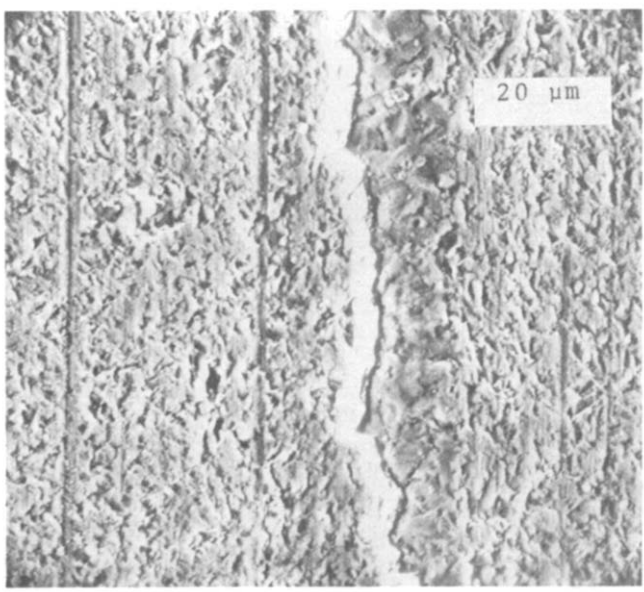

Fig. 8. Tensile surface of a control sample: 341 MPa. The crack runs along the longitudinal axis of the specimen and had an overall length in excess of 4·5 mm.

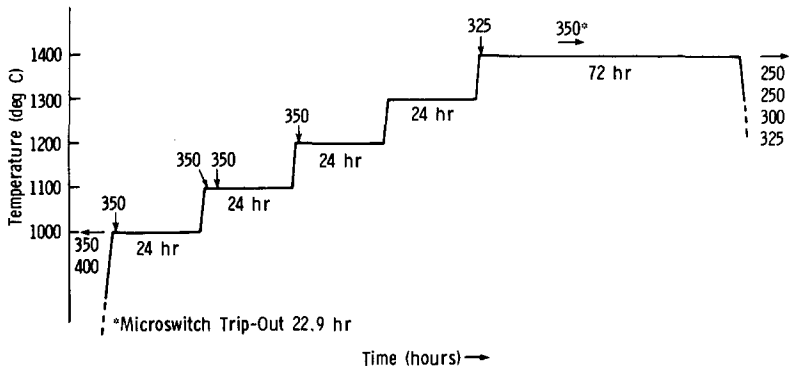

Fig. 9. Stepped temperature stress rupture results.

Twelve specimens were tested via the stepped temperature stress rupture (STSR) procedure and the results are shown in Fig. 9. Two specimens failed on loading with applied stresses of 350 and 400 MPa. Four specimens survived the complete cycle with applied stresses of 250 (2), 300 (1), and 325 MPa (1) and one specimen survived intact at 350 MPa when an inadvertent microswitch trip shut the furnace down after 22·9 h at 1400°C. The five remaining specimens, with applied stresses of 325 (1) and 350 MPa (4) failed in a time-dependent manner at 1000, 1100, 1200, and 1400°C. Permanent deformation of the five survivors was negligible (<0·1% strain). The retained strengths of the four survivors were surprisingly consistent at 401, 448, 402, and 400 MPa for the 250, 250, 300, and

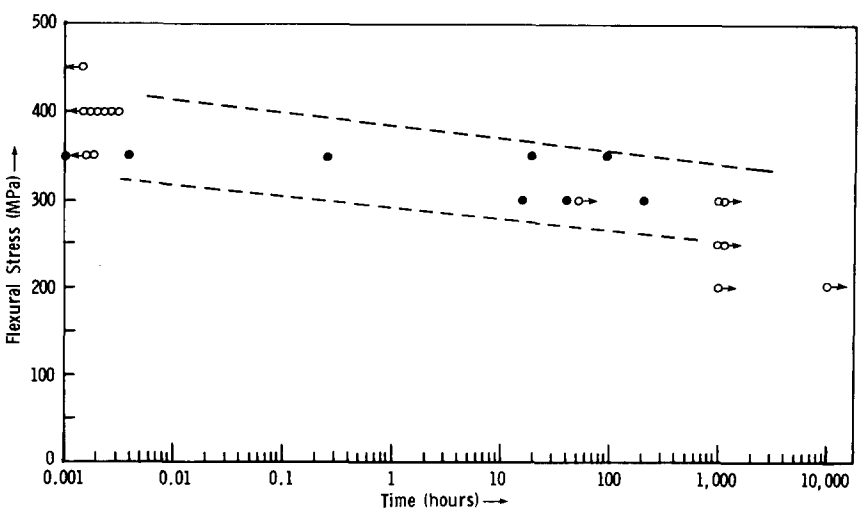

Fig. 10. Flexural stress rupture at 1200°C. The boundary lines approximate the scatter.

350 MPa STSR applied stresses, respectively. The retained strengths are appreciably higher than the reference room temperature strengths (346 MPa average). This may be due either to a flaw healing process or crack blunting.[6]

Twenty-four specimens were tested at 1200°C in the stress rupture experiments (Fig. 10). Nine failed on loading at applied stresses of 350 (2), 400 (6) and 450 MPa (1). Five specimens survived 1000 h at stresses of 200 (1), 250 (2), and 300 MPa (2). One specimen survived 300 MPa for 52·5 h when the furnace malfunctioned and shut down. All surviving specimens had negligible permanent deformation ($\leq 0{\cdot}1\%$ strain) indicating an excellent creep resistance. The retained strengths for the 1000 h survivors were 362, 403, 433, 524 and 524 MPa for the 200, 250, 250, 300 and 300 MPa stress rupture applied stresses, respectively. One specimen which was loaded to 200 MPa survived 10 000 h without failure. Its retained strength at room temperature was 417 MPa and it fractured from a sintering defect. There was only a slight weight change in the specimen since the oxide layer which formed was only 5 μm thick. The retained strengths of all 1200°C survivors were greater than the average room temperature strength. The remaining eight specimens failed in a time-dependent manner from 0·001 h to 210·5 h at applied stresses of 300 and 350 MPa. A static fatigue limit may exist between 200 and 250 MPa.

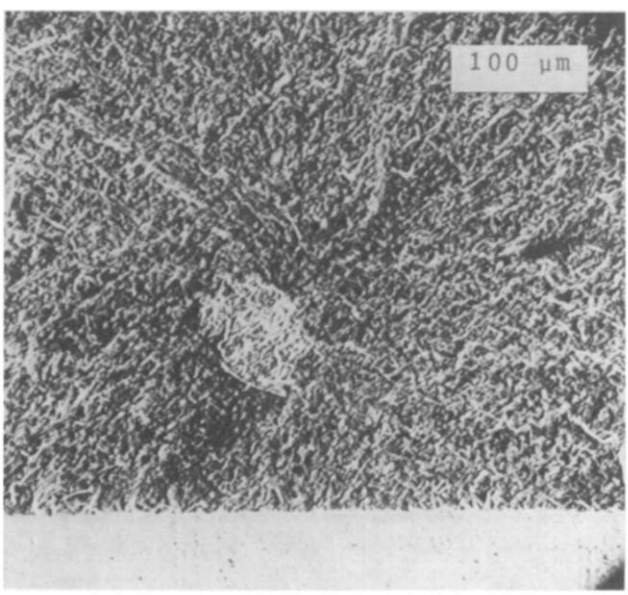

Fig. 11. Fracture surface of a failure on loading during a stress rupture test: 350 MPa. The flaw is a porous area away from the tensile surface.

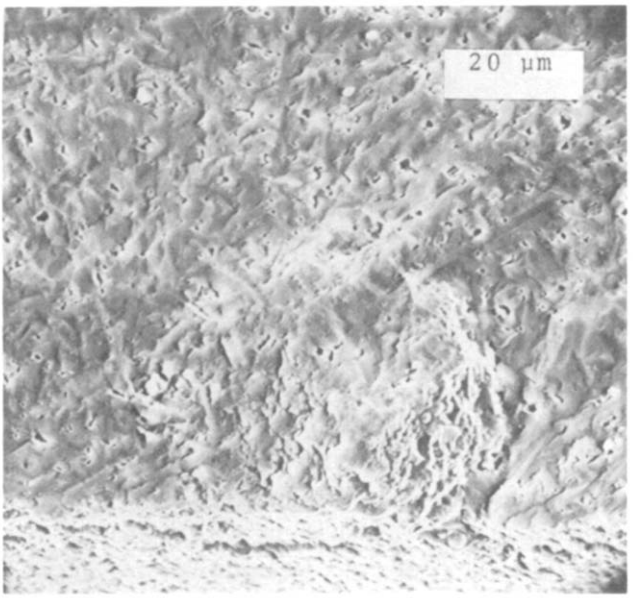

Fig. 12. Fracture surface of a time-dependent failure during a stress rupture test: 300 MPa, $t = 210$ h. Failure occurred at a surface-connected porous area.

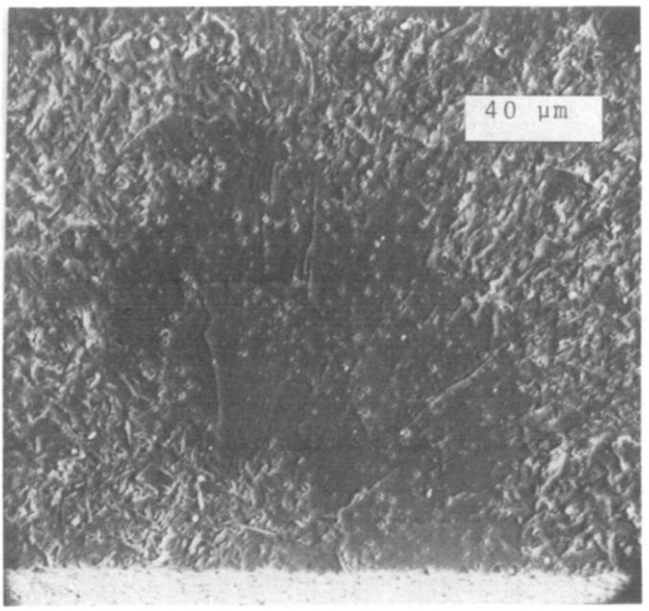

Fig. 13. Fracture surface of a time-dependent failure during a STSR test: 325 MPa, 0·4 h at 1400°C. Failure occurred due to the porous area at the surface which is coincident with a large grain.

The boundary lines on the stress rupture plot (Fig. 10) were drawn to approximate the scatter. None of the specimen fracture surfaces showed any signs of slow crack growth.

The fracture surface characteristics of the stress rupture and STSR time-dependent failures appear identical to those of the fast fracture specimens. The strength-limiting flaws for the failure on loading specimens are volume distributed and are agglomerates (Fig. 11), porous zones, or large grains. The time-dependent failures occurred *exclusively* from surface connected porosity (Figs 12 and 13). This porosity was often an area of small interconnected porosity and not necessarily a discrete void.

5. DISCUSSION

The β-silicon carbide material is subject to static fatigue failure over the 1000–1400°C temperature range for applied flexural stresses of 300–350 MPa, which is at least 85% of the reference fast fracture stress. The scatter in the time to failure of identically loaded specimens was up to five orders of magnitude. The good strength retention at high temperature and the fatigue resistance findings of this study are consistent with earlier reports.[7–10] Double torsion experiments on this material failed to detect any evidence of a time-dependent failure process.[17] That time-dependent failure can occur from surface-connected porous zones, as shown in this report, underscores the desirability of using stress rupture testing.

Although this form of silicon carbide is nominally the β-form, the strength-limiting flaws, the favorable creep and static fatigue resistance, and the enhanced strength of survivors are very similar to results on the sintered α-form of a commercial silicon carbide (Carborundum Corporation, Niagara Falls, New York).[19–21] Indeed, the two materials share a susceptibility of time-dependent failure to primarily surface connected defects, which suggests a stress corrosion phenomenon. Controlled atmosphere experiments would be valuable in clarifying this but were beyond the scope of this screening study.

6. CONCLUSIONS

The sintered β-silicon carbide tested for this program is of a limited production scale and may not necessarily be identical with research laboratory-produced earlier vintages. The Vickers and Knoop microhardness and the Vickers fracture toughness are lower than previously published

data.[7] The room temperature flexural strength is somewhat lower than reported.[9–10]

The intrinsic flaw populations are generally agglomerates and porous zones with a few large grains, inclusions, and process cracks. These flaws are all volume distributed, however. Time-dependent failures occurred only from surface-connected porous zones. There may be an effective stress rupture limit at 1000 h of approximately 250 MPa (~70% of the fast fracture reference strength) at 1200°C. Time-dependent failures occurred throughout the 1000–1400°C temperature range.

The C-scan promises to become a simple, powerful and effective quality control test to find not only large property variations within a tile or component but microstructural variations and severe flaw locations. More in-depth work must be done on the latter two topics for different materials and more complex shapes.

ACKNOWLEDGEMENT

This research was sponsored by the Advanced Materials Development Program Office of Transportation Systems, US Department of Energy IEA DE-AI05-840R 21411 with DOE's Oak Ridge Operation.

APPENDIX

Notation

V_L Longitudinal velocity
d_i Thickness of ith block
t_i Time of flight of ith block
E_i Elastic modulus of ith block
ρ_i Density of ith block
v_i Poisson's ratio for ith block
E_0 Elastic modulus at theoretical density
P Porosity
b Porosity correction factor
ρ_{TH} Theoretical density

The ultrasonic longitudinal wave propagation time C-scan maps point-by-point the wave propagation time through a material. The general equation for the longitudinal wave velocity is:

$$V_L = \frac{2d}{t} = \left[\frac{E}{\rho}\frac{(1-v)}{(1+v)(1-2v)}\right]^{1/2} \tag{A1}$$

which solving for the propagation time becomes

$$t = 2d\rho^{1/2}E^{-1/2}\left[\frac{(1+v)(1-2v)}{(1-v)}\right]^{1/2} \tag{A2}$$

where d, ρ, E, and v are the tile thickness, material density, elastic modulus, and Poisson's ratio, respectively.

The C-scan shown in Fig. 1 shows that (discounting wave distortion at the edges) the wave propagation time, or fly time, increases by approximately 5% from the edge to the center of the tile. Because of this large variation in fly time, it was decided to cut five rectangular blocks through the center of the tile to find the effect of the local material properties on the fly time.

The tile as supplied had a thickness increase from the edge to the center of 1·5%. The five blocks had their densities measured (Archimedes method) and were ultrasonically evaluated for the elastic modulus and Poisson's ratio. The data are shown in Table A1.

TABLE A1
Densities and Sonic Properties of the Machined Blocks

Block i	*Density* $\rho/Mg\,m^{-3}$	ρ_i/ρ_{TH}	*Porosity* P	*Elastic modulus* E/GPa	E_i/E_0	*Poisson's ratio* v
1	3·10	0·967	0·033	404·0	0·907	0·17
2	3·07	0·956	0·044	389·6	0·875	0·16
3	3·05	0·951	0·049	384·4	0·863	0·16
4	3·06	0·954	0·046	388·3	0·872	0·16
5	3·11	0·968	0·032	405·9	0·911	0·16

$\rho_{TH} = 3{\cdot}21\,Mg\,m^{-3}$.
$E_0 = 445\,GPa$.

A decrease in the density corresponding to a decrease in the elastic modulus from the edge to the center of the tile is readily apparent. This relationship, as described by Rice,[22] between the elastic modulus and porosity yields a porosity correction factor, b, of 3·1 and 2·8 for the exponential and linear equations, respectively, assuming an elastic modulus at zero porosity of 445 GPa.* There is no apparent trend in Poisson's ratio versus density through the tile.

This brief analysis does not take into account any secondary microstructure effects on the material properties such as grain size. It was assumed that the porosity is related to the change in theoretical density ($P = 1 - \rho/\rho_{TH}$).

* $E/E_0 = e^{-3{\cdot}1P}$ and $E/E_0 = 1{-}2{\cdot}8P$.

The combined effects of the material properties from block 1 to 3 on the C-scan show a change of +4·0% in the fly time. Using the local properties of the blocks with eqn (A2), the change in fly time is +3·6%. This shows an outstanding agreement even though the 'local' properties are still averages themselves.

A breakdown on change in property required to cause an *increase* in the fly time is:

increased thickness:	major contribution
decreased density	major contribution
decreased elastic modulus:	minor–major contribution
decreased Poisson's ratio:	negligible contribution

Note that the decrease in elastic modulus accompanies the decrease in density which will decrease the fly time.

REFERENCES

1. Prochazka, S. and Charles, R. J., Strength of boron doped hot pressed silicon carbide, *Am. Ceram. Soc. Bull.*, **52**(12) (1973), 885–91.
2. Prochazka, S., Strength of silicon carbide, in *Ceramics for High Performance Applications*, Eds J. Burke, A. Gorum and R. Katz, Brook Hill Publishing Co., Chestnut Hill, Massachusetts, USA, 1974, 239–52.
3. Prochazka, S., Abnormal grain growth in polycrystalline SiC, in *Silicon Carbide—1973*, Proceedings of the Third International Conference on Silicon Carbide, Miami, Florida, September 1973.
4. Prochazka, S. and Charles, R., Strength and microstructure of dense hot pressed silicon carbides, in *Fracture Mechanics of Ceramics*, Vol. 2, Eds R. Bradt, D. Hasselman, and F. Lange, Plenum Press, New York, 1974, 579–98.
5. Prochazka, S., Johnson, C. A. and Giddings, R. A., Atmosphere effects in sintering of silicon carbide, in *Proceedings of International Symposium on Factors in Densification and Sintering of Oxide and Non-Oxide Ceramics*, Eds S. Somiya and S. Saito, Association for Science Documents Information, Tokyo Institute of Technology, Tokyo, Japan, October 1978, 366–81.
6. Johnson, C. A., Crack blunting in sintered SiC, in *Fracture Mechanics of Ceramics*, Vol. 3, Eds R. Bradt, D. Hasselman and F. Lange, Plenum Press, New York, 1978, 99–111.
7. GEC, *Sintride Sintered Silicon Carbide*, General Electric Silicon Carbide Products Operations Brochure, Houston, Texas, 1983.
8. Trantina, G. G. and Johnson, C. A., Subcritical crack growth in boron-doped SiC, *J. Am. Ceram. Soc.*, **58**(7–8) (1975), 344–5.
9. Larsen, D. *Property Screening and Evaluation of Ceramic Turbine Materials*, US Air Force Technical Report AFML-TR79-4188, October 1979.
10. Larsen, D. and Adams, J., *Property Screening and Evaluation of Ceramic Turbine Materials*, US Air Force Technical Report AFWAL TR83-4141, April 1984.

11. US Army MIL-STD-1942(MR), *Flexural Strength of High Performance Ceramics at Ambient Temperature.*
12. Tracy, C. A., Unpublished work, Army Materials and Mechanics Research Center, 1984.
13. Quinn, G. D., *Guide to the Construction of a Simple 1500°C Test Furnace.* Army Materials and Mechanics Research Center, AMMRC TR83-1, January 1983, NTIS ADA 125636.
14. Quinn, G. D., *Characterization of Turbine Ceramics after Long Term Environmental Exposure*, Army Materials and Mechanics Research Center, AMMRC TR80-15, April 1980, NTIS ADA 117463.
15. Quinn, G. D. and Katz, R. N., Stepped temperature stress rupture testing of silicon based ceramics, *Am. Ceram. Soc. Bull.*, **57**(11) (1978), 1057–8.
16. Marshall, D. B. and Evans, A. G., Reply to Comment on 'Elastic/plastic indentation damage in ceramics: the median radial crack system', *Comm. Am. Ceram. Soc.*, **14**(12) (1981), C182–3.
17. Evans, A. G. and Lange, F., Crack propagation and fracture in silicon carbide, *J. Mater. Sci.*, **10** (1975), 1659–64.
18. Larsen, D., *Property Screening and Evaluation of Ceramic Turbine Engine Materials*, US Air Force/IITRI Contract F33615-75C-5196 Interim Report No. 7, March 1979.
19. Quinn, G. D. and Katz, R. N., *Time Dependence of the High Temperature Strength of Sintered Alpha Silicon Carbide*, Army Materials and Mechanics Research Center, AMMRC TN79-5, June 1979.
20. Quinn, G. D., *Stress Rupture of Sintered Alpha Silicon Carbide*, Army Materials and Mechanics Research Center, AMMRC TN81-4, December 1981.
21. Quinn, G. D. and Katz, R. N., Time dependent high temperature strength of sintered α-SiC, *J. Am. Ceram. Soc.*, **63**(1–2) (1980), 117–19.
22. Rice, R. W., Microstructural dependence of mechanical behavior of ceramics, in *Treatise of Materials Science and Technology*, Vol. II, Ed. R. K. MacCrone, Academic Press Inc., New York, 1977, 203–30.

Received 15 October 1985; accepted 16 December 1985